JOC The Journal of Organic Chemistry

Article

pubs.acs.org/joc

β-Functionalized Push−Pull *opp*-Dibenzoporphyrins

R. G. Waruna Jinadasa,[†] Yuanyuan Fang,[‡] Siddhartha Kumar,[†] Allen J. Osinski,[§] Xiaoqin Jiang,[‡] Christopher J. Ziegler,[§] Karl M. Kadish,*[,‡] and Hong Wang*[,†]

[†]Department of Chemistry and Biochemistry, Miami University, 701 E High Street, Oxford, Ohio 45056, United States

[‡]Department of Chemistry, University of Houston, Houston, Texas 77204-5003, United States

[§]Department of Chemistry, University of Akron, Akron, Ohio 44325, United States

Supporting Information

ABSTRACT: The synthesis of a series of β-functionalized push−pull dibenzoporphyrins was realized. These porphyrins display subtle push−pull effects, demonstrating the exceptional tunability of their electronic and electrochemical properties. The UV−vis spectra of these porphyrins show unique absorption patterns with shouldered Soret bands and extra absorptions in the Q-band region. Stronger electron-withdrawing groups display more significant bathochromic shifts of the Soret bands. The fluorescence spectra of these porphyrins show strong near-IR emission bands (600−850 nm). In particular, fluorescence quenching effect was observed for pyridyl carrying push−pull porphyrin **4c** in the presence of an acid. TFA titration study of **4c** using UV−vis and fluorescence spectroscopy reveals that the fluorescence quenching can be mainly attributed to the protonation of the pyridyl groups of **4c**. The versatile synthetic methods developed in this work may open a door to access a large number of functionalized organic materials that are currently unavailable. The structure−property studies provided in this work may provide useful guidelines for the design of new generations of materials in dye-sensitized solar cells, in nonlinear optical applications, as fluorescence probes, as well as sensitizers for photodynamic therapy.

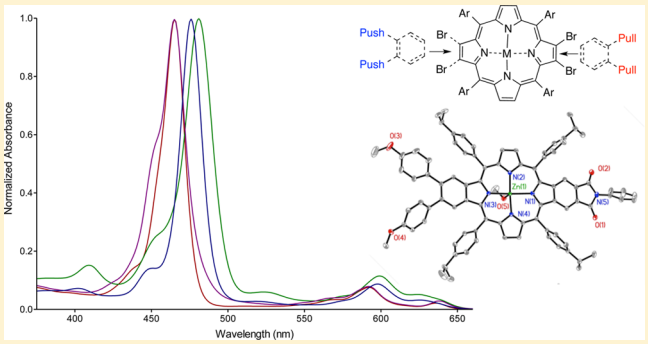

INTRODUCTION

Push−pull porphyrins carrying both an electron-donating (push) and an electron-withdrawing group (pull) have been a topic of long-lasting research interest owing to their potential applications in organic electronics, optoelectronics and photonics.[1−5] Breakthroughs in the development of push−pull porphyrins were not made until 2011 when dye-sensitized solar-cells (DSSCs), which were based on a class of push−pull porphyrins bearing a diarylamine donor group and an ethynylbenzoic acid acceptor (linker) group at the porphyrin *meso*-positions (Figure 1), achieved a record-high solar-to-electric-power-conversion efficiency (η = 12.3%).[6] This exciting achievement has drastically changed the traditional poor-performance profile of porphyrins in DSSC.

Intense research efforts have been devoted to developing push−pull porphyrins since then,[7−9] and even more exciting results have been obtained,[10−23] demonstrating the huge potentials of push−pull porphyrins in this area. Almost all reported push−pull porphyrins are functionalized at the porphyrin *meso*-positions, and there are only a few examples for β-functionalized push−pull porphyrins in the literature.[16,24,25] *Meso*- and β-functionalization at the porphyrin periphery is expected to have a different effect on their electronic and optophysical properties (Figure 1). Given the remarkable advances achieved with *meso*-functionalized push−

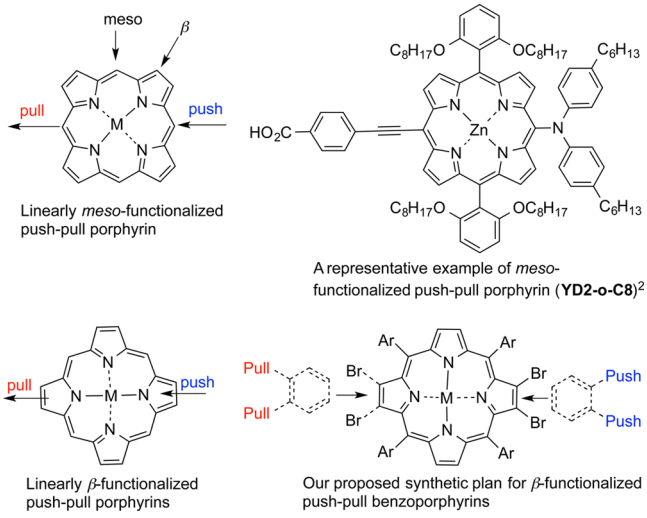

Figure 1. Illustration of *meso*- and β-functionalized push−pull porphyrins.

Received: September 1, 2015
Published: November 18, 2015

DOI: 10.1021/acs.joc.5b01906
J. Org. Chem. 2015, 80, 12076−12087

Scheme 1. Preparation of Push–Pull *opp*-Dibenzoporphyrins

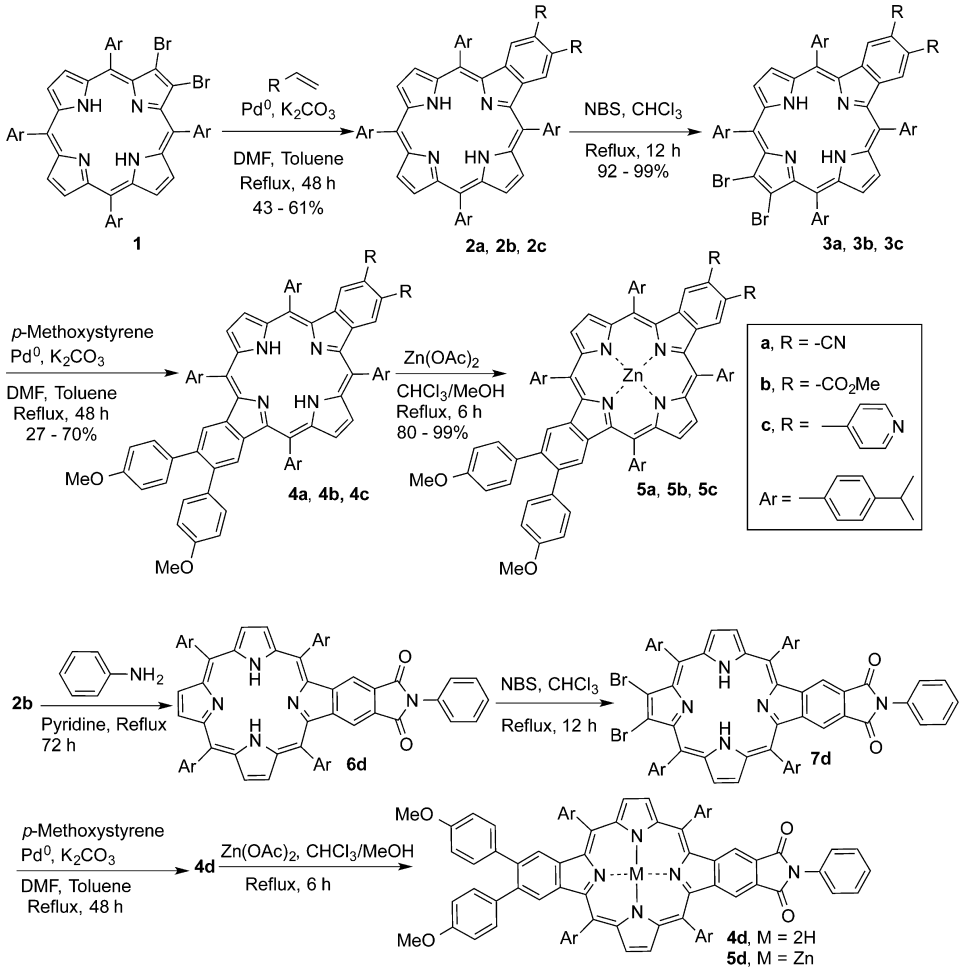

pull porphyrins in recent years, *β*-functionalized push–pull porphyrins hold potential to make new breakthroughs. In order to achieve this, we believe the key is to develop concise and versatile synthetic methods to access *β*-functionalized push–pull porphyrins. Recently we have developed a Pd^0 catalyzed cascade reaction for the synthesis of benzoporphyrins.[26] This cascade reaction allows the possibility to introduce a wide range of functional groups to the porphyrin *β*, *β*′-positions. We wished to take advantage of the versatility of this reaction in conjunction with the bromination chemistry of porphyrins[27−31] and to develop a new synthetic route that can potentially lead to a large variety of *β*-functionalized push–pull porphyrins (Figure 1). Herein, we report the synthesis and characterization of a series of push–pull *opp*-dibenzoporphyrins where the push group features the *p*-methoxyphenyl group and the pull groups possess variable electron-withdrawing abilities.

RESULTS AND DISCUSSION

Synthesis of the Materials. *π*-Extended porphyrins, in which one or more aromatic rings are fused to the porphyrin *β*, *β*′-positions, possess a unique set of electronic and photophysical properties, and thus constitute of an attractive research field.[32−35] However, *π*-extended porphyrins are notoriously difficult to synthesize. Functionalization of *π*-extended porphyrins is very challenging. In this work, we show that through the cooperation of a palladium catalyzed cascade reaction[26] with the bromination chemistry of porphyrin,[28,31] push–pull *opp*-dibenzoporphyrins (**4a**–**4d** and **5a**–**5d**) are readily prepared (Scheme 1).

The Pd^0 catalyzed cascade reaction involves three sequential reactions: the Heck reaction, electro-cyclization of alkenes, and aromatization. The synthesis of these push–pull *opp*-dibenzoporphyrins started from 2,3-dibromoporphyrin **1**, which was obtained from literature-reported procedures.[26] The reaction of dibromoporphyrin **1** with a substituted alkene in the presence of an in situ formed Pd^0 catalyst led to ready installation of a benzene ring at the porphyrin *β*,*β*′-positions, affording the monobenzoporphyrins **2a**–**2c** carrying two electron-withdrawing groups. Bromination of **2a**–**2c** using NBS in $CHCl_3$ generated the 12,13-dibromobenzoporphyrin **3a**–**3c**. The fused benzene ring of **2a**–**2c** helps to lock the aromatic delocalization pathway of the free base porphyrins making it possible to regioselectively brominate **2a**–**2c** at the *β*, *β*′-positions of the crossed pyrrole ring. **3a**–**3c** reacted with *p*-methoxystyrene through the Pd^0 catalyzed cascade reaction to give the free base push–pull *opp*-dibenzoporphyrins **4a**–**4c**. Zinc insertion into **4a**–**4c** led to the push–pull zinc *opp*-dibenzoporphyrins **5a**–**5c**. The push–pull *opp*-dibenzoporphyrins **4d** and **5d** bearing a cyclic imide group were prepared from **2b** possessing two vicinal ester groups. The vicinal ester groups in **2b** were converted into cyclic imide using aniline in the presence of pyridine to afford **6d** in good yield. Subsequent regioselective bromination of **6d** produced bromo-benzoporphyrin **7d**. Then it was reacted with *p*-methoxystyene via Pd^0

DOI: 10.1021/acs.joc.5b01906
J. Org. Chem. 2015, 80, 12076−12087

catalyzed cascade reaction to generate **4d**. The insertion of zinc into **4d** gave **5d**. All of these compounds have been characterized using ^{1}H and ^{13}C NMR spectroscopy, and LDI-TOF MS spectrometry (see the SI). Single crystals suitable for X-ray crystallography were obtained for **5d** through slow vapor dispersion of MeOH into a $CHCl_3$ solution of **5d**. The crystal structure of **5d** (CCDC, 1404127) shows that the porphyrin ring is essentially planar (Figure 2). The fused benzene ring carrying the imide group lies in the plane of the porphyrin core. The other fused benzene is slightly deviated from the plane of the porphyrin core.

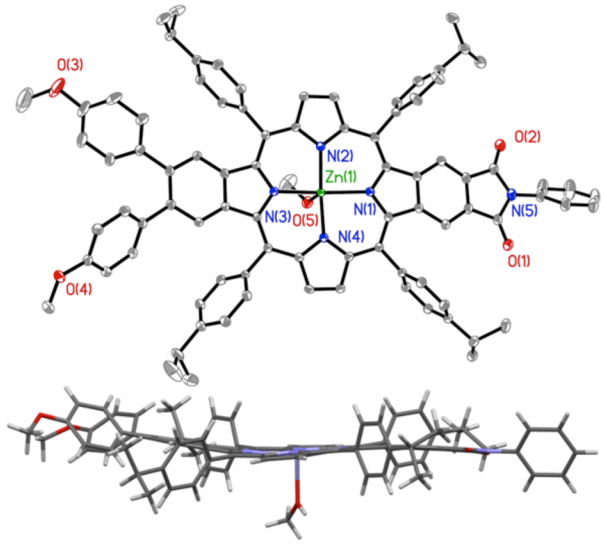

Figure 2. X-ray crystal structure of **5d**. Top: top view with 35% thermal ellipsoids. Hydrogen atoms have been omitted for clarity. Bottom: side view.

Electronic and Photophysical Properties. Push–pull *opp*-dibenzoporphyrins **5a–5d** and **4a–4d** bear the same *p*-methoxyphenyl donating groups on one fused benzene ring of the porphyrin, and the groups with variable electron-withdrawing abilities are attached on the other fused benzene ring at the opposite β,β'-positions of the porphyrin. The UV–vis absorption spectra of **5a–5d** and **4a–4d** in DCM are compiled in Figure 3 and Figure S1 (see the SI), respectively. **4b**, which possesses moderate electron-withdrawing ester groups, displays a broad Soret band at 448 nm and four Q bands in the range of 500–750 nm.

Upon switching to much stronger electron-withdrawing cyano groups (**4a**), the Soret band is red-shifted by 8 to 456 nm; the Q bands of **4a** are also red-shifted relative to those of **4b**. These data demonstrate a stronger push–pull effect of **4a** than **4b**. Simply converting the vicinal ester groups of **4b** to a cyclic imide group in **4d** significantly red shifts the Soret band by 12 to 460 nm. The Q bands of **4d** are also red-shifted relative to those of **4b**. Such a remarkable substituent effect displayed by **4d** demonstrates the strong electron-withdrawing ability of the planar cyclic imide group, which is more efficiently conjugated to the porphyrin π-system than the two free-rotating ester groups. On the other hand, the pyridyl bearing **4c** shows blue-shifted Soret and Q bands relative to those of **4b**, **4a**, and **4d**. UV–vis absorption bands of **5a**, **5b**, and **5d** are red-shifted relative to those of the corresponding free base porphyrins **4a**, **4b**, and **4d** by 5–8 nm, and exhibit a similar trend of spectral change as observed for **4a**, **4b**, and **4d**. In sharp contrast, the pyridyl bearing **5c** shows bathochromic-shifted Soret and Q bands relative to those of **5a** and **5b**, displaying a reversed trend. It is remarkable that the Soret band of **5c** is red-shifted by 17 nm relative to that of its free base **4c**. Such a large shift of the Soret band upon metalation indicates that a different process has occurred during metalation (see the SI Figure S2 for comparison of the UV–vis spectra of pyridyl containing **2c** and zinc-**2c**). UV–vis spectra of **5a–5d** were then measured in pyridine (Figure 4).

While **5a**, **5b**, and **5d** all display large bathochromically shifted Soret bands (up to 14 nm) with significantly different

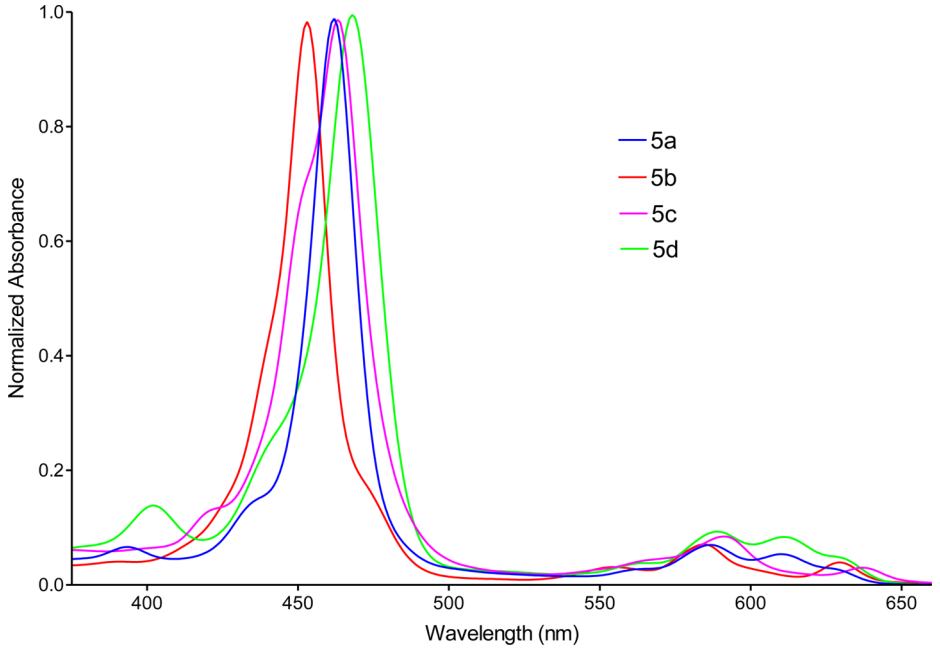

Figure 3. Normalized UV–vis spectra of **5a–5d** in CH_2Cl_2 (**5a**, 6.99×10^{-6} M; **5b**, 7.45×10^{-6} M; **5c**, 6.35×10^{-6} M; **5d**, 3.15×10^{-6} M).

DOI: 10.1021/acs.joc.5b01906
J. Org. Chem. 2015, 80, 12076–12087

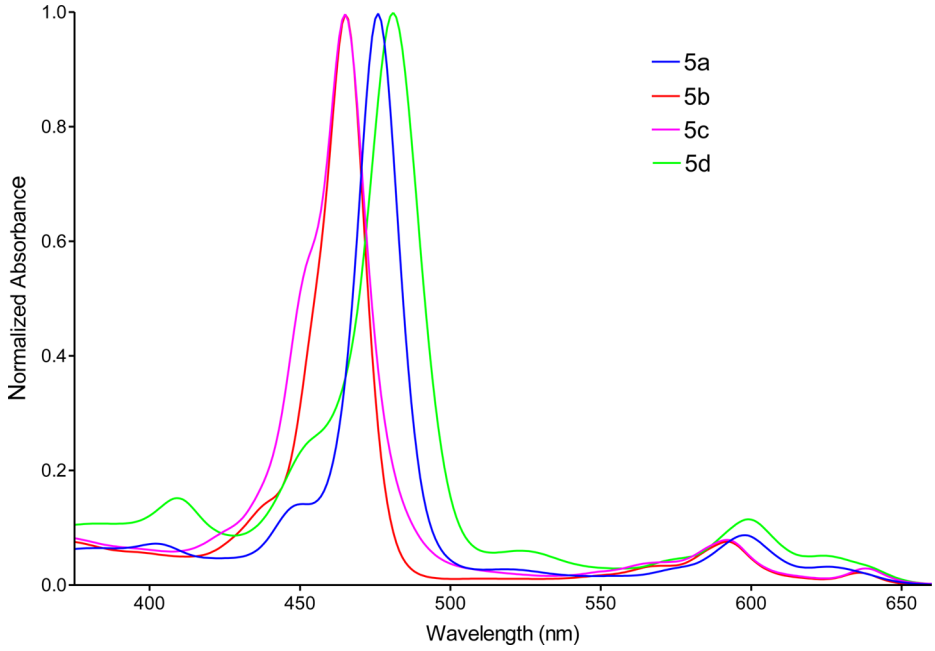

Figure 4. Normalized UV−vis spectra of **5a**−**5d** in pyridine.

absorption patterns at the Q-band region (500−700 nm) in pyridine as compared with those in CH_2Cl_2, those of **5c** remain more or less similar to only a 2 nm red-shift of the Soret band. These data suggest that the pyridyl substituents of one **5c** molecule are able to coordinate to the central zinc of another **5c** molecule in CH_2Cl_2, and may possibly form a coordination framework (Figure 5).

Overall, the trend observed in the UV−vis spectra of **5a**−**5d** in pyridine is similar to that of **4a**-**4d** in CH_2Cl_2. For better comparison, UV−vis spectra in CH_2Cl_2 and pyridine were overlaid for **5a**−**5d** in Figures S5−S8 in the SI. The UV−vis absorption spectra of the synthesized push−pull *opp*-dibenzoporphyrins possess several unique features: (1) the Soret bands are shouldered; (2) an additional weaker absorption shows in the range of 380−405 nm; (3) extra Q bands are observed in the range of 500−650 nm, noting that four and two Q bands are expected for free base porphyrins and metalated porphyrins, respectively. These features become especially pronounced for the more strongly push−pull **4a**, **5a**, **4d**, and **5d**. For example, zinc porphyrin **5d** shows four Q bands, both in CH_2Cl_2 and in pyridine. These features of the UV−vis spectra can be partially explained by breakage of the symmetry from D_{4h} to C_{2v}. However, we speculate that intramolecular charge transfers/electronic communication involving the push and pull groups, the porphyrin core and the central metal are likely to exist in these porphyrins.

Steady state fluorescence spectroscopy of **4a**−**4d** and **5a**−**5d** was measured in CH_2Cl_2 (Figure 6, and Figure S3 in the SI). All the push−pull *opp*-dibenzoporphyrins except **4d** show two emission bands. **4d** exhibits multiple overlapping emission bands. In particular, **4a**−**4d** display strong and broad near IR emission bands in the range of 600−850 nm. The fluorescence spectra of **4a**−**4d** and **5a**−**5d** reflect similar trends as observed in their UV−vis absorption spectra. Since **4c** and **5c** carry basic pyridyl groups, we measured their fluorescence spectroscopy in acidic conditions by treating the porphyrin with gradual addition of TFA in CH_2Cl_2 solution (Figure 7 and Figure S4 in the SI). It is interesting that upon treating with TFA, the

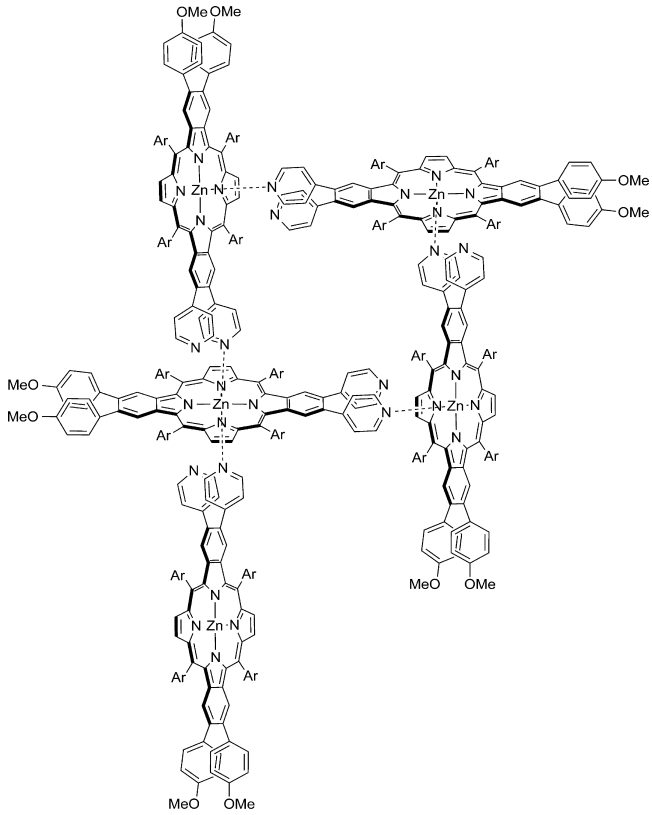

Figure 5. Proposed coordination framework of **5c** in CH_2Cl_2. Note, the framework is expected to exist as a mixture of oligomers.

fluorescence intensities of **4c** and **5c** are both significantly decreased. While almost fully quenching of the band at 676 nm was observed for **4c** when >2.75 equiv of TFA was added, the fluorescence band at 749 nm of **4c** only displayed decreased intensity with minimal shift when TFA < 1.83 equiv. The band shift and the change for the band shape become more significant when TFA > 2.75 equiv, but the intensity of the

DOI: 10.1021/acs.joc.5b01906
J. Org. Chem. 2015, 80, 12076−12087

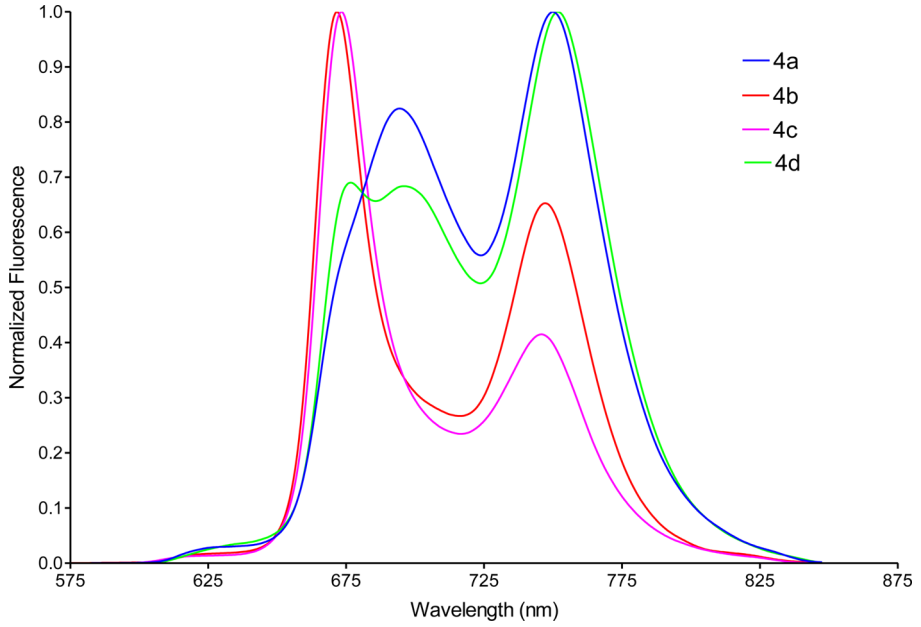

Figure 6. Normalized fluorescence spectra of **4a**–**4d** in CH_2Cl_2 at excitation wavelength 470 nm.

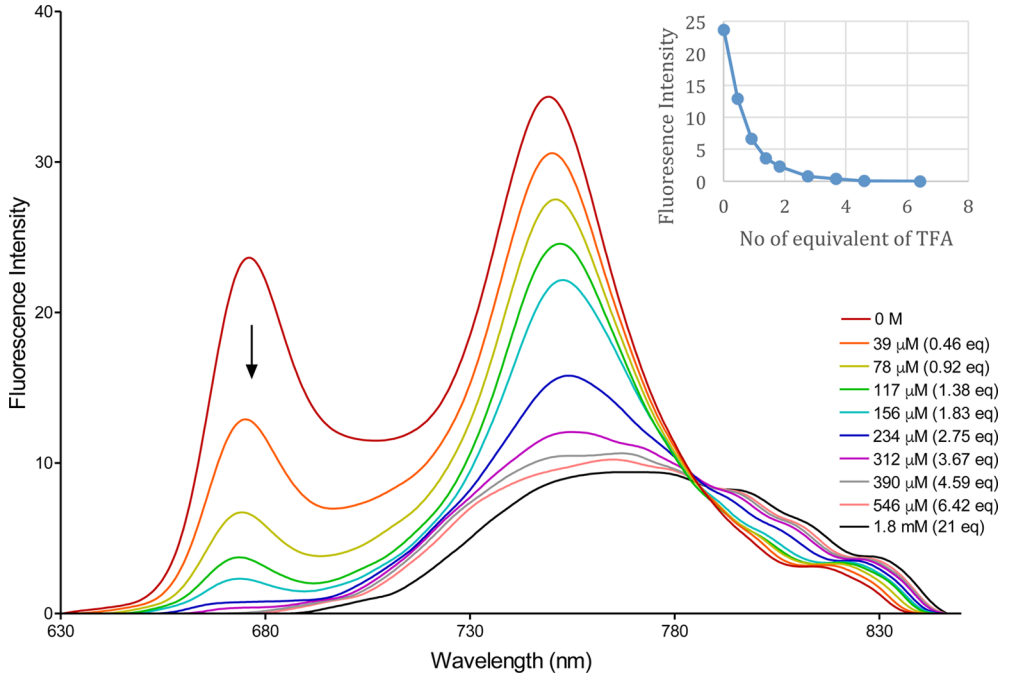

Figure 7. Fluorescence emission changes (λ_{ex} = 612 nm) of **4c** (8.5×10^{-5} M) upon addition of TFA in DCM at 25 °C. (Inset) Fluorescence intensity changes of **4c** at λ = 676 nm as a function of equivalent of TFA.

band decreased less significantly. The fluorescence bands of **5c** displayed a similar trend. These phenomena are not observed for other free base and zinc(II) porphyrins. In order to better understand these phenomena, **4c** (Figure 8) was titrated with TFA, and the UV–vis absorption spectroscopy was used to monitor the titration process. Upon addition of <~2.0 equiv of TFA, the intensity of the Soret band of **4c** decreased, but the absorption intensity of the Q-band at 612 nm increased slightly (see insets in Figure 8). On the other hand, both the shifts of the Soret band and the Q bands were neglectable. When >2.0 equiv of TFA was added, more significant shifts of the Soret band and the Q bands were observed. When large excess of TFA was added, the UV–vis absorption bands displayed significant bathochromic shifts. The Soret band was much broadened and the Q bands were much enhanced. These data suggest that, upon treatment with TFA, protonation of the basic pyridyl moieties of **4c** occurs first followed by protonation of the free base porphyrin.[36] Based on these data, it can be concluded that the fluorescence quenching observed for **4c** in the presence of TFA is mainly caused by the protonation of pyridyl groups of **4c**.

The absorption and emission data are summarized in Table 1 for **5a**–**5d**.

Electrochemical Properties. Electrochemistry of the Zn(II) porphyrins **5a** to **5d** was investigated by cyclic voltammetry in CH_2Cl_2 and pyridine containing 0.1 M

DOI: 10.1021/acs.joc.5b01906
J. Org. Chem. 2015, 80, 12076–12087

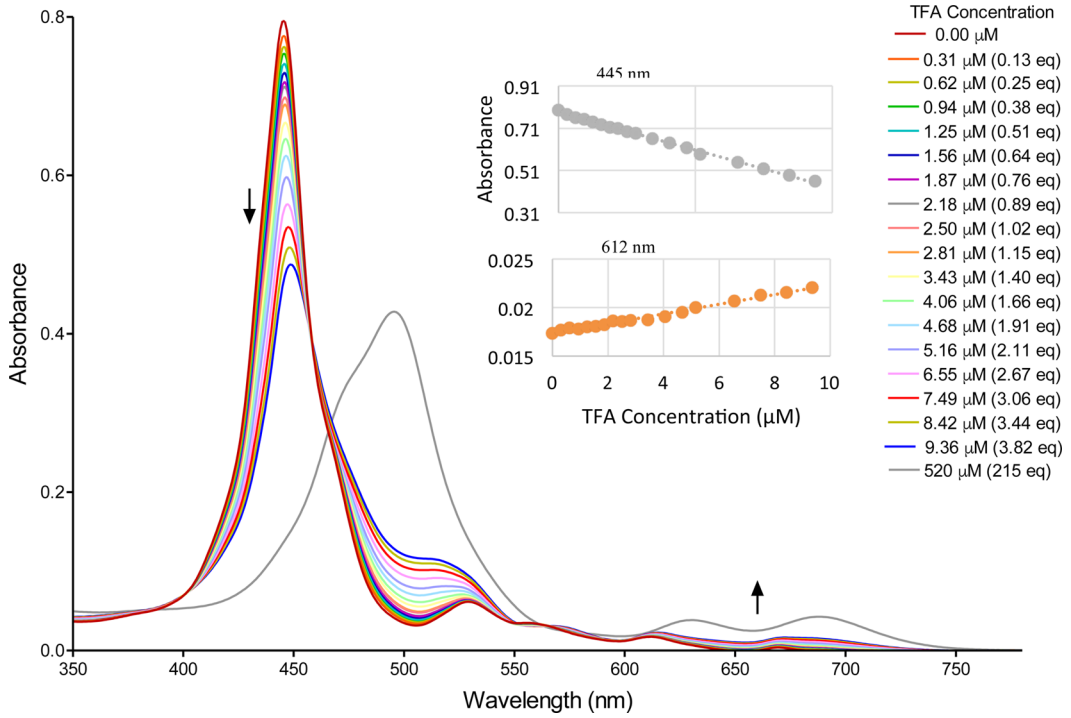

Figure 8. UV−vis absorbance changes of **4c** (2.45×10^{-6} M) upon addition of TFA in DCM at 25 °C. (Inset) Absorbance changes of **4c** at λ = 445 nm and λ = 612 nm as a function of TFA concentration.

Table 1. Absorption and Emission Data of 5a−5d

	λ_{max} B (nm)			emission (nm)		
compounds	in CH_2Cl_2	in Pyr	in $CHCl_3$ (log ε)	in CH_2Cl_2	in Pyr	Φ F[a] in DMF
5a	462	476	468 (5.35)	635, 697	641, 710	0.028
5b	453	465	453 (5.38)	632, 696	640, 705	0.021
5c	463	465	458 (5.39)	636, 698	641, 707	0.035
5d	468	481	474 (5.35)	634, 700	643, 713	0.027

[a]Fluorescence quantum yields were calculated using TPP (λ_{ex} = 601 nm, ΦF = 0.11 in DMF)[37] as a standard in DMF at 25 °C.

TBAP. Each compound exhibits two oxidations and two or three reductions in CH_2Cl_2 as shown in Figure 9.

The two oxidations and the first reduction of each porphyrin are reversible. The second reduction of **5c** is also reversible but this process is irreversible for compounds **5a**, **5d**, and **5b** in CH_2Cl_2. The first two electron additions are porphyrin ring centered and generate a porphyrin π-anion radical and dianion but the dianion formed during the second reduction is not stable in the case of **5a**, **5b**, or **5d** and is converted to a phlorin anion via a homogeneous chemical reaction described in earlier publications for related compounds.[38−40] The chemically generated phlorin anion is electroactive and can be further reduced at more negative potentials to a phlorin dianion. It can also be reoxidized to give back the neutral porphyrin at a peak potential of −0.38 to −0.40 V. Taking compound **5a** as an example, three reductions are observed in CH_2Cl_2, the first at $E_{1/2}$ = −1.26 V, the second at E_{pc} = −1.65 V, and the third at $E_{1/2}$ = −1.91 V, as seen in Figure 9. The reoxidation peak at E_{pa} = −0.38 V is coupled to the second reduction. A third reduction is not observed for porphyrins **5d** or **5b** due to the fact that this reaction occurs at $E_{1/2}$ values more negative than the solvent potential limit of CH_2Cl_2. A third reduction is also not seen for **5c**, which is more difficult to reduce than the other three porphyrins and lacks a reoxidation peak at −0.38 V. The first reduction of **5c**, which has the proposed coordination framework shown in Figure 5, is located at $E_{1/2}$ = −1.42 V which is 130−160 mV more negative than $E_{1/2}$ for reduction of **5a**, **5b**, or **5d** ($E_{1/2}$ = −1.26 to −1.29 V) in the same solvent. This large negative shift in reduction potential for **5c** is consistent with a coordination between the Zn(II) center of one porphyrin molecule and the pyridyl group(s) from another as schematically shown in Figure 5. Changing from the nonbinding solvent CH_2Cl_2 to the strongly binding solvent pyridine results in a change from four coordinate Zn(II) to five coordinate Zn(Py) for compounds **5a**, **5d**, and **5b** and the occurrence of two well-defined reversible reductions for all four porphyrins (Figure 10). The $E_{1/2}$ for first reduction in pyridine ranges from −1.19 to −1.30 V and the second from −1.61 to −1.79 V. A chemical reaction following the second reduction of **5c**, **5b**, and **5d** is not observed in pyridine (as is the case in CH_2Cl_2) due to the smaller proton concentration in this solvent. In addition, the fact that **5b** and **5c** exhibit exactly the same reduction potentials in pyridine suggests the same five-coordinate Zn(Py) form of the porphyrin in this solvent. The first oxidation of **5a** in CH_2Cl_2 occurs at $E_{1/2}$ = 0.78 V while $E_{1/2}$ = 0.72 V for **5b**, **5c**, and **5d**. The second oxidation of **5a** and **5c** are identical within experimental error while the $E_{1/2}$ values for oxidation of **5b** and **5d** are exactly identical, as seen in Figure 9. Thus, conversion of the vicinal esters in **5b** to the cyclic imide in **5d** does not shift the oxidation potentials, but replacing the moderately electron-withdrawing ester groups of **5b** with strongly electron-withdrawing cyano groups in **5a** positively shifts both the first and the second oxidations by 60 and 40 mV, respectively.

DOI: 10.1021/acs.joc.5b01906
J. Org. Chem. 2015, 80, 12076−12087

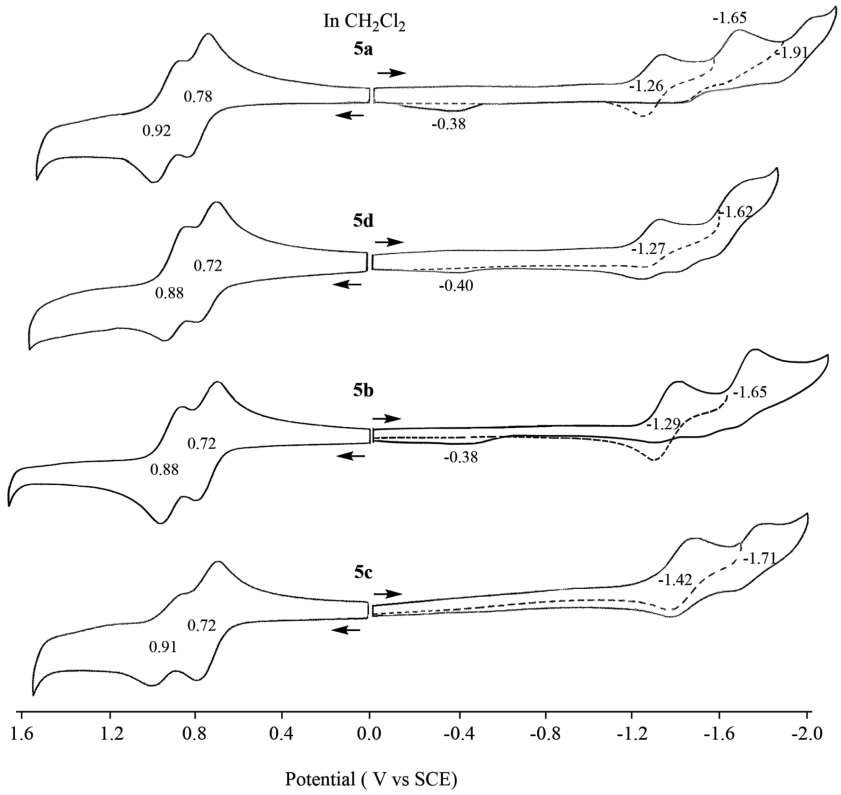

Figure 9. Cyclic voltammograms of investigated dibenzo zinc porphyrins in CH_2Cl_2, 0.1 M TBAP.

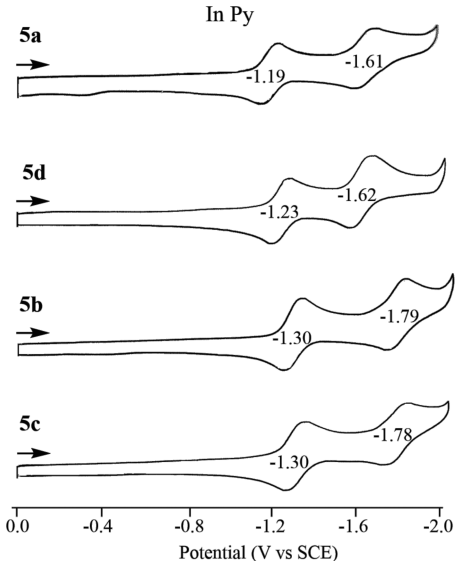

Figure 10. Cyclic voltammograms of investigated zinc dibenzoporphyrins in pyridine, 0.1 M TBAP.

While **5b** and **5c** exhibit almost the same reduction potentials, the first and the second reduction potentials of **5a** are shifted positively in pyridine by 110 mV and 180/170 mV, respectively, relative to those of **5b** and **5c** (see Figure 10). The incorporation of two cyano groups in the push−pull *opp*-dibenzoporphyrin **5a** shifts both the oxidation and the reduction potentials positively as compared to the other porphyrins in CH_2Cl_2. Overall, a variation in the strength of the electron-withdrawing groups makes a bigger impact on the reduction potentials than the oxidation potentials for these *β*-functionalized push−pull *opp*-dibenzoporphyrins.

The electrochemical data are summarized in Table 2. The electrochemical HOMO−LUMO energy gaps, calculated from reversible potentials for the first oxidation and first reduction in CH_2Cl_2 follows the order: **5d** (1.99) < **5b** (2.01) < **5a** (2.04) < **5c** (2.14). On the other hand, the HOMO−LUMO gap calculated from UV−vis absorption data is in the order of **5d** < **5c** < **5a** < **5b**. It is not clear to us what factors cause the discrepancy between these two energy gaps.

DFT Calculation. DFT calculations were conducted for **5a**−**5d** to provide insights into the electronic and electrochemical properties of these compounds (Figure 11). The electronic density on the HOMO and the LUMO+1 of these

Table 2. Electrochemical Data of 5a−5d

compounds	E_{ox} (V) (DCM)	E_{red} (V) (DCM)	E_{red} (V) (DCM)	ΔE (V) (DCM)	E_{0-0} [a] (eV) (DCM)	E_{0-0} [a] (eV) (Pyr)	ΔE_{cal} [b]
5a	0.78	−1.26	−1.19	2.04	2.0493	2.0342	2.61
5b	0.72	−1.29	−1.30	2.01	2.0561	2.0578	2.60
5c	0.72	−1.42	−1.30	2.14	2.0459	2.0544	2.56
5d	0.72	−1.27	−1.23	1.99	2.0375	2.0259	2.61

[a] E_{0-0} was determined from the intersection of normalized absorption and emission spectra. [b] HOMO−LUMO energy gaps were calculated by DFT calculations with B3LYP/6-31G(d) level.

DOI: 10.1021/acs.joc.5b01906
J. Org. Chem. 2015, 80, 12076−12087

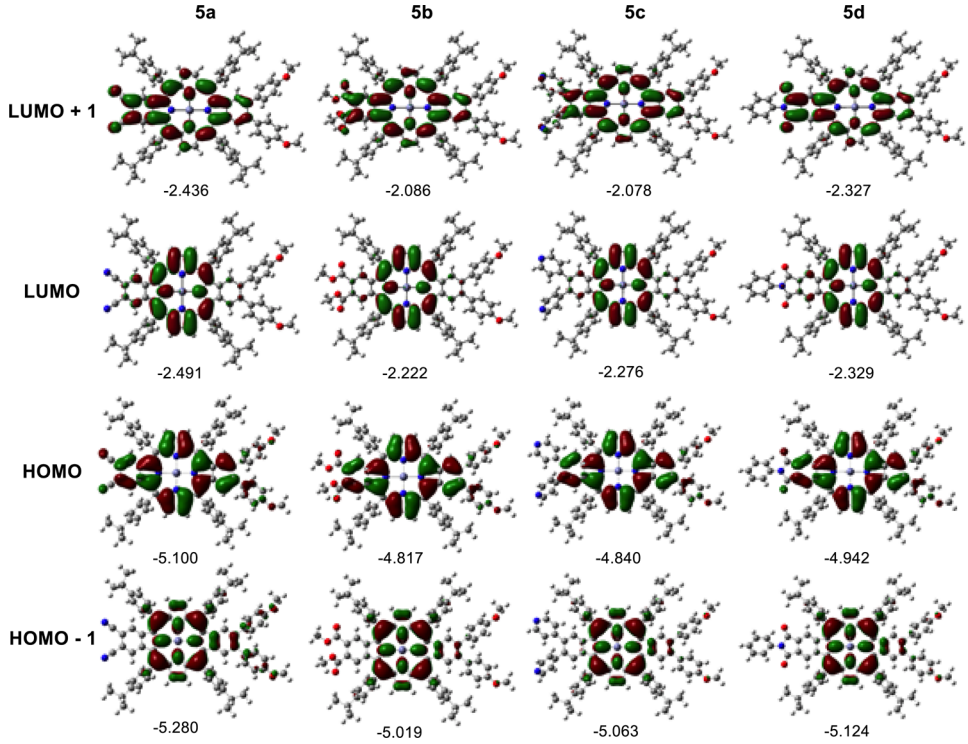

Figure 11. Calculated HOMOs, LUMOs, and energy levels (eV) for **5a**−**5d** (B3LYP/6-31G(d)).

porphyrins is significantly distributed over the porphyrin ring and the two fused benzene rings. The participation of the two pyrroles bearing no substituents in the LUMO+1 is much less than that of the two neighboring pyrroles bearing substituents, suggesting some "locking effect" due to the fusion of the two benzene rings.

The electron density of the LUMO and the HOMO−1 of these porphyrins is mainly located at the π-systems of the porphyrin core. The introduction of a strongly electron-withdrawing group (i.e., −CN) slightly increases the participation of the fused benzene ring bearing the electron-withdrawing group in the LUMO and the fused benzene ring bearing the electron-donating group in the HOMO−1. On the other hand, the HOMO and LUMO+1 involve both the porphyrin core and the two fused benzene rings. The introduction of a strongly electron-withdrawing group (i.e., −CN) enhances the participation of the electron-withdrawing groups in both the HOMO and LUMO+1. It is notable that the electron-donating *p*-methoxyphenyl group is only minimally involved in the HOMO and HOMO−1 of these porphyrins due to their restricted rotation forcing the benzene rings to adopt a perpendicular position relative to the porphyrin plane.

CONCLUSIONS

In summary, the synthesis of a novel class of push−pull *opp*-dibenzoporphyrins is described in this work. The versatile synthetic methods demonstrated in this work open a new door for functionalizing porphyrins. The electronic and electrochemical properties of these push−pull *opp*-dibenzoporphyrins are susceptible to changes in substituents suggesting their easy tunability. For example, the replacement of the two vicinal ester groups (**5b**) both with two strongly electron-withdrawing cyano groups (**5a**) and with a moderately electron-withdrawing cyclic imide group (**5d**) can significantly narrow their HOMO−LUMO energy gaps. On the other hand, the substituent effects on the energy levels of their frontier orbitals are different. While the energy levels for the HOMO and HOMO−1 of the imide carrying **5d** remain identical with those of the ester carrying **5b**, those of **5a** are both moderately lowered relative to those of **5b**. It should also be noted that the pyridyl carrying **4c** exhibits fluorescence quenching in the presence of TFA, a phenomenon that is not observed in other free base porphyrins.

These push−pull *opp*-dibenzoporphyrins display interesting UV−vis absorption spectra and near-IR fluorescence, which can be useful as sensitizers in a number of applications such as dye-sensitized solar cells, nonlinear optical applications, and photodynamic therapy. They may also serve as model systems to study intra- and intermolecular electron transfer. The structure−property study has shown that the incorporation of a strong electron-withdrawing group has significant impact on the electronic and electrochemical properties of the porphyrins. On the other hand, the electron-donating group, i.e., *p*-methoxyphenyl group, shows a limited influence on the electronic and electrochemical properties of the porphyrins. This is likely due to that the two vicinal aryl rings are forced to adopt a dominant position perpendicular to the porphyrin ring due to the restricted rotation of these two rings. As such, electron-donation through resonance is not in play for these two methoxy groups, leading to minimal push effect. Future direction for the development of β-functionalized push−pull benzoporphyrins will lie in the development of electron-donating groups that can conjugate more effectively to the porphyrin π-system, so that more efficient electronic communications engaging the electron-donating group, the electron-withdrawing group and the porphyrin π-system can be achieved.

EXPERIMENTAL SECTION

All solvents were analytical reagent grade, and were used without further purification unless otherwise noted. Analytical TLC's were

DOI: 10.1021/acs.joc.5b01906
J. Org. Chem. 2015, 80, 12076−12087

performed on silica TLC plates. Column chromatography was performed on silica gel (40−63 μm). All NMR spectra were recorded on 500 MHz (^{1}H NMR), 125 MHz (^{13}C NMR)) spectrometer. All samples were prepared in $CDCl_3$, MeOD or *d*-pyridine and chemical shifts were referenced to $CHCl_3$ at 7.26 ppm for ^{1}H NMR and referenced to the $CDCl_3$ at 77.0 ppm for ^{13}C NMR. Mass spectra were obtained on MALDI-TOF mass spectrometer. UV−vis spectra were recorded on UV−vis-NIR spectrometer in CH_2Cl_2, $CHCl_3$ or pyridine.

Cyclic voltammetry was carried out at 298 K. A homemade three-electrode cell consisted of a glassy carbon-working electrode, a platinum counter electrode, and a homemade saturated calomel reference electrode (SCE) was used for cyclic voltammetric measurements. The SCE was separated from the bulk of the solution by a fritted glass bridge of low porosity, which contained the solvent/supporting electrolyte mixture. High purity N_2 was used to deoxygenate the solution and kept over the solution during each electrochemical and spectroelectrochemical experiment. Dibromo porphyrin **1** was synthesized according to previously published procedure.[26]

Procedure for the Synthesis of Monobenzoporphyrin 2a. Dibromoporphyrin **1** (100 mg, 0.11 mmol) and K_2CO_3 (30 mg, 0.22 mmol) were added to a Schlenk flask and dried under vacuum. The vacuum was released under argon to allow the addition of dry THF (20 mL). The mixture was then degassed via four freeze−pump−thaw cycles before the addition of $Pd[P(tBu)_3]_2$ (15 mg, 0.03 mmol) and acrylonitrile (0.13 mL, 2.0 mmol). The Schlenk flask was then sealed and heated at 50 °C for 40 h. The solvent was removed and the residue was redissolved in toluene. Pd/C (20 mg) was added and the resulting mixture was refluxed for 24 h. The reaction mixture was diluted with EtOAc and was washed with water for 3 times. The organic layer was removed solvent under reduced pressure. The resulting residue was subjected to silica column chromatography (CH_2Cl_2/cyclohexane). The band containing the desired porphyrin **2a** was collected and was recrystallized from CH_2Cl_2/MeOH.

*5,10,15,20-Tetrakis[4-(1-methylethyl)phenyl]benzo[b]-porphinato-2^2,2^3-dicarbonitrile (**2a**).* $C_{62}H_{54}N_6$ purple crystalline solid (mp >300 °C), 35 mg, 0.04 mmol, 40%. UV−vis (CH_2Cl_2) λ_{max} (rel. inten.) 441 nm (1.000), 531 (0.046), 606 (0.009) 667 (0.001); ^{1}H NMR (500 MHz, $CDCl_3$) δ 9.01 (s, 4H), 8.78 (s, 2H), 8.16 (d, J = 7.9 Hz, 4H), 8.09 (d, J = 7.8 Hz, 4H), 7.75 (d, J = 7.8 Hz, 4H), 7.66 (d, J = 7.8 Hz, 4H), 7.21 (s, 2H), 3.38 (dt, J = 13.8, 6.9 Hz, 2H), 3.30 (dt, J = 13.7, 6.9 Hz, 2H), 1.65 (d, J = 6.9 Hz, 12H), 1.61−1.53 (m, 12H), −2.65 (s, 2H). ^{13}C NMR (126 MHz, $CDCl_3$) δ 156.1, 150.8, 148.7, 146.6, 143.0, 139.2, 139.0, 138.9, 138.9, 134.8, 134.7, 133.6, 130.5, 128.7, 128.4, 126.2, 125.0, 121.8, 118.6, 116.8, 110.7, 34.5, 34.1, 24.6, 24.3. IR (neat, diamond ATR): see Figure S11, SI; HRMS (ESI) m/z: $[M + H]^+$ Calcd for $C_{62}H_{55}N_6$ 883.4488; Found 883.4507. MS (MALDI-TOF) m/z: 882.354 $[M]^+$.

General Procedure for the Synthesis of Benzoporphyrins 2b−2c. Dibromoporphyrin **1** (100 mg, 0.11 mmol), palladium acetate (2 mg, 0.01 mmol), triphenylphosphine (6 mg 0.02 mmol), and K_2CO_3 (30 mg 0.22 mmol) were added to a Schlenk flask and dried under vacuum. The vacuum was released under argon to allow the addition of dry DMF (10 mL) and dry toluene (10 mL). The mixture was then degassed via four freeze−pump−thaw cycles before the vessel was purged with argon again. Then the vinyl precursor (20-fold excess) was added. The Schlenk flask was sealed and was heated to reflux for 48 h. After 48 h, the reaction mixture was diluted with EtOAc and was washed with water 3 times. The organic layer was removed solvent under reduced pressure. The residue was subjected to silica column chromatography (CH_2Cl_2/MeOH). The band containing the desired porphyrins **2b−2c** was collected and was recrystallized from CH_2Cl_2/MeOH.

*Dimethyl-5,10,15,20-tetrakis[4-(1-methylethyl)phenyl]benzo[b]-porphinato-2^2,2^3-dicarboxylate (**2b**).* $C_{64}H_{60}N_4O_4$ purple crystalline solid (mp >300 °C), 58 mg, 0.06 mmol, 61%. UV−vis (CH_2Cl_2) λ_{max} (rel. inten) 433 nm (1.000), 525 (0.051), 600 (0.016), 660 (0.002); ^{1}H NMR (500 MHz, $CDCl_3$) δ 8.94 (d, J = 4.9 Hz, 2H), 8.90 (d, J = 4.8 Hz, 2H), 8.75 (s, 2H), 8.19−8.07 (m, J = 16.4, 7.8 Hz, 8H), 7.70 (d, J = 7.8 Hz, 4H), 7.62 (d, J = 7.8 Hz, 4H), 7.46 (s, 2H), 3.89 (s, 6H), 3.34 (dt, J = 13.9, 6.9 Hz, 2H), 3.27 (dt, J = 13.8, 7.0 Hz, 2H), 1.61 (d, J = 6.9 Hz, 12H), 1.55 (d, J = 6.9 Hz, 12H), −2.61 (s, 2H). ^{13}C NMR (126 MHz, $CDCl_3$) δ 168.7, 149.7, 148.4, 143.0, 139.4, 139.2, 134.8, 134.0, 133.8, 129.0, 128.0, 128.0, 125.9, 125.5, 124.9, 121.3, 118.0, 52.5, 34.3, 34.1, 24.5, 24.3. IR (neat, diamond ATR): see Figure S12, SI; HRMS (ESI) m/z: $[M + H]^+$ Calcd for $C_{64}H_{61}N_4O_4$ 949.4693; Found 949.4703. MS (MALDI-TOF) m/z: 948.373 $[M]^+$.

*5,10,15,20-Tetrakis[4-(1-methylethyl)phenyl]-2^2,2^3-di(pyridine-4-yl)benzo[b]porphyrin (**2c**).* $C_{70}H_{62}N_6$ purple crystalline solid (mp >350 °C), 45 mg, 0.04 mmol, 46%. UV−vis (CH_2Cl_2) λ_{max} (rel. inten.) 434 nm (1.000), 523 (0.050), 599 (0.014); ^{1}H NMR (500 MHz, $CDCl_3$) δ 8.96 (d, J = 4.7 Hz, 2H), 8.88 (d, J = 4.7 Hz, 2H), 8.77 (s, 2H), 8.48 (d, J = 5.1 Hz, 4H), 8.22−8.11 (m, 8H), 7.72−7.59 (m, 8H), 7.26 (s, 2H), 6.97 (d, J = 5.4 Hz, 4H), 3.43−3.14 (m, 4H), 1.57 (d, J = 6.9 Hz, 12H), 1.49 (d, J = 6.9 Hz, 12H), −2.55 (s, 2H). ^{13}C NMR (126 MHz, $CDCl_3$) δ 149.5, 149.4, 148.4, 139.9, 139.3, 135.2, 134.7, 133.9, 133.7, 128.0, 127.7, 127.1, 125.9, 124.9, 124.8, 121.4, 117.4, 34.2, 34.1, 24.3, 24.29. IR (neat, diamond ATR): see Figure S13, SI; HRMS (ESI) m/z: $[M + H]^+$ Calcd for $C_{70}H_{63}N_6$ 987.5114; Found 987.5125. MS (MALDI-TOF) m/z: 986.419 $[M]^+$.

General Procedure for the Synthesis of Dibromoporphyrins 3a−3c. Monobenzoporphyrin **2a−2c** (1 equiv) and *N*-bromosuccinimide (2.5 equiv) was dissolved in dry chloroform. The mixture was reflux for 6−12 h. The reaction progress was monitored with UV−vis spectroscopy. After the reaction was completed, the reaction mixture was washed with aqueous NaOH, water, and brine. The organic layer was removed solvent under reduced pressure, and the resulting residue was recrystallized in CH_2Cl_2/MeOH to afford the pure compound **3a−3c**.

*12,13-Dibromo-5,10,15,20-tetrakis[4-(1-methylethyl)phenyl]-benzo[b]porphinato-2^2,2^3-dicarbonitrile (**3a**).* $C_{62}H_{52}Br_2N_6$ brown solid (mp >280 °C), 37 mg, 0.04 mmol, 91%. UV−vis (CH_2Cl_2) λ_{max} (rel. inten.) 448 nm (1.000), 540 (0.056), 616 (0.014), 684 (0.014); ^{1}H NMR (500 MHz, $CDCl_3$) δ 8.90 (d, J = 3.6 Hz, 2H), 8.82 (d, J = 3.6 Hz, 2H), 8.14−8.02 (m, 8H), 7.73 (d, J = 7.8 Hz, 4H), 7.64 (d, J = 7.8 Hz, 4H), 7.18 (s, 2H), 3.39−3.30 (m, 2H), 3.30−3.22 (m, 2H), 1.61 (d, J = 6.9 Hz, 12H), 1.53 (d, J = 6.8 Hz, 12H), −2.69 (s, 2H). ^{13}C NMR (126 MHz, $CDCl_3$) δ 151.0, 149.8, 148.2, 147.6, 142.7, 140.4, 139.8, 138.2, 138.11, 135.4, 134.0, 130.3, 129.9, 128.4, 126.3, 125.7, 125.1, 121.7, 118.7, 116.6, 111.2, 34.5, 34.2, 24.5, 24.4. HRMS (ESI) m/z: $[M + H]^+$ Calcd for $C_{62}H_{52}Br_2N_6$ 1041.2678; Found 1041.2677. MS (MALDI-TOF) m/z: 1041.174 $[M + H]^+$.

*Dimethyl-12,13-dibromo-5,10,15,20-tetrakis[4-(1-methylethyl)-phenyl]benzo[b]porphinato-2^2,2^3-dicarboxylate (**3b**).* $C_{64}H_{58}Br_2N_4O_4$ brown solid (mp >250 °C), 55 mg, 0.05 mmol, 96%. ^{1}H NMR (500 MHz, $CDCl_3$) δ 8.85 (d, J = 3.8 Hz, 2H), 8.74 (d, J = 4.0 Hz, 2H), 8.17−8.04 (m, J = 7.4, 5.5 Hz, 8H), 7.69 (d, J = 7.7 Hz, 4H), 7.63 (d, J = 7.8 Hz, 4H), 7.39 (s, 2H), 3.86 (s, 6H), 3.38−3.10 (m, J = 27.0, 13.7, 6.8 Hz, 4H), 1.58 (d, J = 6.9 Hz, 12H), 1.53 (d, J = 6.9 Hz, 12H), −2.59 (s, 2H). ^{13}C NMR (126 MHz, $CDCl_3$) δ 168.4, 149.9, 149.8, 149.5, 147.3, 142.7, 140.8, 138.9, 138.6, 138.4, 135.4, 134.2, 129.4, 129.4, 127.8, 126.0, 125.6, 125.3, 124.1, 121.3, 118.1, 52.5, 34.3, 34.2, 24.4, 24.4. HRMS (ESI) m/z: $[M + H]^+$ Calcd for $C_{64}H_{58}Br_2N_4O_4$ 1107.2887; Found 1107.2924 MS (MALDI-TOF) m/z: 1107.336 $(M+H)^+$.

*12,13-Dibromo-5,10,15,20-tetrakis[4-(1-methylethyl)phenyl]-2^2,2^3-di(pyridine-4-yl)benzo[b]porphyrin (**3c**).* $C_{70}H_{60}Br_2N_6$ brown solid (mp >280 °C), 42 mg, 0.04 mmol, 92%. UV−vis (CH_2Cl_2) λ_{max} (rel. inten.) 444 nm (1.000), 536 (0.058), 610 (0.018), 678 (0.004); ^{1}H NMR (500 MHz, $CDCl_3$) δ 8.89 (d, J = 4.4 Hz, 2H), 8.74 (d, J = 4.5 Hz, 2H), 8.47 (d, J = 4.8 Hz, 4H), 8.14 (dd, J = 18.6, 7.7 Hz, 8H), 7.72−7.60 (m, 8H), 7.20 (s, 2H), 6.96 (d, J = 4.9 Hz, 4H), 3.42−3.14 (m, J = 20.7, 13.7, 6.7 Hz, 4H), 1.56 (d, J = 6.9 Hz, 12H), 1.48 (d, J = 6.9 Hz, 12H), −2.52 (s, 2H). ^{13}C NMR (126 MHz, $CDCl_3$) δ 150.5, 149.8, 149.5, 149.4, 149.3, 147.1, 141.9, 140.9, 139.1, 138.7, 138.4, 135.5, 135.4, 134.0, 129.5, 127.5, 127.0, 126.0, 125.6, 124.8, 124.0, 121.4, 117.5, 34.2, 34.2, 24.4, 24.3. HRMS (ESI) m/z: $[M + H]^+$ Calcd for $C_{70}H_{61}Br_2N_6$ 1145.3304; Found 1145.3335. MS (MALDI-TOF) m/z: 983.403 $[M-2Br]^+$.

DOI: 10.1021/acs.joc.5b01906
J. Org. Chem. 2015, 80, 12076−12087

General Procedure for the Synthesis of Dibenzoporphyrins 4a−4c. Dibromoporphyrin **3a−3c** (1 equiv), palladium acetate (0.01 equiv), triphenylphosphine (0.02 equiv) and K_2CO_3 (2 equiv) were added to a Schlenk flask and dried under vacuum. The vacuum was released under argon to allow the addition of dry DMF (10 mL) and dry toluene (10 mL). The mixture was then degassed via four freeze−pump−thaw cycles before the vessel was purged with argon again. *p*-methoxystyrene (15-fold excess) was added. The Schlenk flask was sealed and was heated to reflux for 72 h. The mixture was then diluted with EtOAc and was washed with water for 3 times. The organic layer was removed under reduced pressure. The resulting residue was subjected to silica column chromatography (CH_2Cl_2/cyclohexane or CH_2Cl_2/MeOH). The bands containing the desired porphyrins **4a** − **4c** were collected and were recrystallized from CH_2Cl_2/MeOH.

*5,10,15,20-Tetrakis[4-(1-methylethyl)phenyl]-12^2,12^3-bis(4-methoxyphenyl)dibenzo [b,l]porphinato-2^2,2^3-dicarbonitrile (**4a**).* $C_{80}H_{68}N_6O_2$ purple crystalline solid (mp >300 °C), 14 mg, 0.012 mmol, 30%. UV−vis (CH_2Cl_2) λ_{max} (log ε) 456 nm (5.61), 541 (4.28), 579 (4.33), 615 (4.11). ^{1}H NMR (500 MHz, $CDCl_3$) δ 8.93 (d, J = 3.8 Hz, 2H), 8.86 (d, J = 4.8 Hz, 2H), 8.15 (d, J = 7.8 Hz, 4H), 8.10 (d, J = 7.8 Hz, 4H), 7.75 (d, J = 7.8 Hz, 4H), 7.67 (d, J = 7.8 Hz, 4H), 7.21 (s, 2H), 7.19 (s, 2H), 6.98 (d, J = 8.5 Hz, 4H), 6.76 (d, J = 8.5 Hz, 4H), 3.84 (s, 6H), 3.37 (dt, J = 13.4, 6.7 Hz, 2H), 3.26 (dt, J = 13.9, 7.0 Hz, 2H), 1.65 (d, J = 6.9 Hz, 12H), 1.50 (d, J = 6.9 Hz, 12H), −2.49 (s, 2H). ^{13}C NMR (126 MHz, $CDCl_3$) δ 158.1, 151.8, 150.7, 149.5, 145.8, 142.2, 140.8, 140.4, 139.3, 138.7, 138.3, 134.5, 133.7, 131.1, 130.3, 128.4, 127.7, 127.0, 126.2, 126.0, 119.3, 118.5, 116.9, 113.3, 110.4, 55.2, 34.5, 34.0, 24.5, 24.3. IR (neat, diamond ATR): see Figure S14, SI; HRMS (ESI) m/z: $[M + H]^+$ Calcd for $C_{80}H_{69}N_6O_2$ 1145.5482; Found 1145.5491. MS (MALDI-TOF) m/z: 1144.470 $[M]^+$.

*Dimethyl-5,10,15,20-Tetrakis[4-(1-methylethyl)phenyl]-12^2,12^3-bis(4-methoxyphenyl)dibenzo[b,l]porphinato-2^2,2^3-dicarboxylate (**4b**).* $C_{82}H_{74}N_4O_6$ purple crystalline solid (mp >300 °C), 12 mg, 0.010 mmol, 40%. UV−vis (CH_2Cl_2) λ_{max} (log ε) 447 nm (5.62), 532 (4.34), 566 (4.08), 612 (3.84). ^{1}H NMR (500 MHz, $CDCl_3$) δ 8.83 (d, J = 3.7 Hz, 2H), 8.79 (d, J = 4.7 Hz, 2H), 8.18−8.08 (m, 8H), 7.69 (d, J = 7.9 Hz, 4H), 7.63 (d, J = 7.9 Hz, 4H), 7.43 (s, 2H), 7.17 (s, 2H), 6.96 (d, J = 8.6 Hz, 4H), 6.73 (d, J = 8.6 Hz, 4H), 3.87 (s, 6H), 3.80 (s, 6H), 3.33 (dt, J = 13.8, 6.9 Hz, 2H), 3.23 (dt, J = 13.8, 6.9 Hz, 2H), 1.60 (d, J = 6.9 Hz, 12H), 1.47 (d, J = 6.9 Hz, 12H), −2.51 (s, 2H). ^{13}C NMR (126 MHz, $CDCl_3$) δ 168.7, 158.1, 150.7, 149.7, 149.3, 147.9, 142.4, 140.8, 139.7, 139.5, 139.2, 138.5, 138.1, 134.8, 133.9, 133.7, 131.1, 128.8, 127.7, 127.2, 126.8, 125.91, 125.87, 125.3, 118.8, 118.2, 113.3, 55.2, 34.3, 34.2, 24.4, 24.3. IR (neat, diamond ATR): see Figure S15, SI; HRMS (ESI) m/z: $[M + H]^+$ Calcd for $C_{82}H_{75}N_4O_6$ 1211.5687; Found 1211.5741. MS (MALDI-TOF) m/z: 1210.538 $[M]^+$.

*5,10,15,20-Tetrakis[4-(1-methylethyl)phenyl]-2^2,2^3-di(pyridine-4-yl)-12^2,12^3-bis(4-methoxyphenyl)dibenzo[b,l]porphyrin (**4c**).* $C_{88}H_{76}N_6O_2$ purple crystalline solid (mp >300 °C), 76 mg, 0.061 mmol, 70%. UV−vis (CH_2Cl_2) λ_{max} (log ε) 445 nm (5.41), 529 (4.32), 612 (3.80), 669 (3.45). ^{1}H NMR (500 MHz, $CDCl_3$) δ 8.81 (s, 4H), 8.44 (d, J = 5.3 Hz, 4H), 8.14 (d, J = 7.9 Hz, 8H), 7.72−7.58 (m, 8H), 7.21 (s, 2H), 7.17 (s, 2H), 7.03−6.88 (m, 4H), 6.73 (d, J = 8.6 Hz, 4H), 3.81 (s, 6H), 3.30−3.17 (m, 4H), 1.52−1.43 (m, 24H), −2.51 (s, 2H). ^{13}C NMR (126 MHz, $CDCl_3$) δ 158.1, 150.5, 149.5, 149.5, 149.3, 148.5, 141.7, 140.8, 139.7, 139.7, 139.2, 138.6, 138.1, 134.9, 134.8, 133.7, 131.1, 128.2, 127.3, 127.2, 126.9, 126.8, 125.9, 125.9, 124.9, 118.3, 118.3, 113.3, 55.2, 34.22, 34.20, 24.3. IR (neat, diamond ATR): see Figure S16, SI; HRMS (ESI) m/z: $[M + H]^+$ Calcd for $C_{88}H_{77}N_6O_2$ 1249.6108; Found 1249.6135 MS (MALDI-TOF) m/z: 1249.525 $[M + H]^+$.

General Procedure for the Synthesis of Zinc Dibenzoporphyrins 5a−5c. Dibenzoporphyrin **4a−4d** (1 equiv) and $Zn(OAc)_2$ (10 equiv) were dissolved in 1:3 MeOH/$CHCl_3$ mixture. The mixture was reflux for 12 h. Reaction completion was monitored with TLC. After completion of the reaction, the solvent was removed. Residue was dissolved in $CHCl_3$ and was washed with water and brine. After removal of the solvent, the product was recrystallized in CH_2Cl_2/MeOH to obtain the pure compound **5a−5d**.

*5,10,15,20-Tetrakis[4-(1-methylethyl)phenyl]-12^2,12^3-bis(4-methoxyphenyl)dibenzo [b,l]porphinato-2^2,2^3-dicarbonitrile, Zinc (**5a**).* $C_{80}H_{66}N_6O_2Zn$ green solid (mp >300 °C), 10 mg, 0.008 mmol, 95%. UV−vis ($CHCl_3$) λ_{max} (log ε) 397 nm (4.23) 468 (5.35), 591 (4.17), 617 (4.05). ^{1}H NMR (500 MHz, $CDCl_3$) δ 8.96 (d, J = 4.7 Hz, 2H), 8.86 (d, J = 4.7 Hz, 2H), 8.08 (d, J = 7.9 Hz, 4H), 8.04 (d, J = 7.9 Hz, 4H), 7.72 (d, J = 7.9 Hz, 4H), 7.64 (d, J = 7.9 Hz, 4H), 7.38 (s, 2H), 7.37 (s, 2H), 6.99 (d, J = 8.6 Hz, 4H), 6.76 (d, J = 8.6 Hz, 4H), 3.82 (s, 6H), 3.35 (dt, J = 13.9, 6.9 Hz, 2H), 3.25 (dt, J = 13.9, 6.9 Hz, 2H), 1.63 (d, J = 7.0 Hz, 12H), 1.50 (d, J = 6.9 Hz, 12H). ^{13}C NMR (126 MHz, $CDCl_3$) δ 158.2, 152.0, 150.5, 149.7, 149.3, 147.1, 141.6, 140.1, 139.7, 139.5, 139.1, 138.7, 134.6, 133.1, 133.0, 132.1, 131.5, 131.2, 131.1, 127.2, 126.0, 125.9, 120.5, 119.5, 117.0, 113.4, 109.5, 55.2, 34.5, 34.2, 24.6, 24.3. IR (neat, diamond ATR): see Figure S20, SI; HRMS (MALDI-TOF) m/z: $[M]^+$ Calcd for $C_{80}H_{66}N_6O_2Zn$ 1206.4539; Found 1206.2983 (see SI for isotopic spectrum). MS (MALDI-TOF) m/z: 1206.416 $[M]^+$.

*Dimethyl-5,10,15,20-tetrakis[4-(1-methylethyl)phenyl]-12^2,12^3-bis(4-methoxyphenyl) dibenzo[b,l]porphinato-2^2,2^3-dicarboxylate, Zinc (**5b**).* $C_{82}H_{72}N_4O_6Zn$ green solid (mp >300 °C), 12 mg, 0.009 mmol, 96%. UV−vis (CH_2Cl_2) λ_{max} (log ε) 453 nm (5.45), 554 (3.92), 585 (4.30), 630 (4.03). ^{1}H NMR (500 MHz, $CDCl_3$) δ 8.83 (d, J = 4.7 Hz, 2H), 8.79 (d, J = 4.6 Hz, 2H), 8.17−8.04 (m, 8H), 7.67 (d, J = 7.8 Hz, 4H), 7.64−7.59 (m, 6H), 7.39 (s, 2H), 7.01 (d, J = 8.5 Hz, 4H), 6.76 (d, J = 8.5 Hz, 4H), 3.90 (s, 6H), 3.83 (s, 6H), 3.34 (dt, J = 13.9, 7.0 Hz, 2H), 3.25 (dt, J = 13.6, 6.8 Hz, 2H), 1.61 (d, J = 6.9 Hz, 12H), 1.50 (d, J = 6.9 Hz, 12H). ^{13}C NMR (126 MHz, $CDCl_3$) δ 168.8, 158.1, 150.9, 149.8, 149.3, 149.0, 145.9, 143.4, 140.6, 140.4, 140.1, 139.1, 138.1, 134.8, 133.3, 133.2, 131.4, 131.2, 131.0, 128.2, 127.0, 125.8, 125.7, 125.7, 119.9, 119.1, 113.3, 55.2, 52.5, 34.3, 34.2, 24.5, 24.4. IR (neat, diamond ATR): see Figure S21, SI; HRMS (MALDI-TOF) m/z: $[M]^+$ Calcd for $C_{82}H_{72}N_4O_6Zn$ 1272.4743; Found 1272.2726 (see SI for isotopic spectrum). MS (MALDI-TOF) m/z: 1272.467 $[M]^+$.

*5,10,15,20-Tetrakis[4-(1-methylethyl)phenyl]-2^2,2^3-di(pyridine-4-yl)-12^2,12^3-bis(4-methoxyphenyl)dibenzo[b,l]porphyrin, Zinc (**5c**).* $C_{88}H_{74}N_6O_2Zn$ green amorphous solid (mp >300 °C), 12 mg, 0.009 mmol, 80%. UV−vis ($CHCl_3$) λ_{max} (log ε) 458 nm (5.39), 588 (4.34), 634 (3.97). ^{1}H NMR (500 MHz, $CDCl_3$) δ 8.82 (s, 4H), 8.45 (d, J = 4.7 Hz, 4H), 8.12−8.04 (m, 8H), 7.62−7.56 (m, 8H), 7.42 (s, 2H), 7.39 (s, 2H), 7.04−6.94 (m 8H), 6.75 (d, J = 7.6 Hz, 4H), 3.79 (s, 6H), 3.30−3.14 (m, 4H), 1.57−1.38 (m, 24H). ^{13}C NMR (126 MHz, $CDCl_3$) δ 158.0, 150.6, 149.9, 149.9, 149.7, 148.9, 148.7, 145.3, 143.5, 141.2, 140.1, 139.4, 137.6, 135.7, 134.9, 134.2, 133.3, 133.2, 131.2, 130.8, 127.1, 126.9, 125.4, 125.4, 124.9, 123.5, 118.9, 118.9, 113.3, 55.1, 34.2, 34.1, 24.4. IR (neat, diamond ATR): see Figure S22, SI; HRMS (ESI) m/z: $[M + 2H]^{2+}$ Calcd for $C_{88}H_{76}N_6O_2Zn$ 656.2660; Found 656.2675. MS (MALDI-TOF) m/z: 1310.533 $[M]^+$.

Procedure for the Synthesis of Monobenzoporphyrin 6d. Monobenzoporphyrin **2c** (57 mg, 0.06 mmol) was desolved in 1:1 mixture of aniline and pyridine (6 mL). Mixture was refluxed for 72h. Reaction was monitored by TLC. After completion of the reaction solvent was removed under vacuum. Residue was recrystallized in MeOH/CH_2Cl_2 and purified via silica column chromatography (CH_2Cl_2/cyclohexane) to obtain compound **6d**.

*5,10,15,20-Tetrakis[4-(1-methylethyl)phenyl]porphinato[2,3-f]-isoindole-1,3(2H)-dione, 2-phenyl (**6d**).* $C_{68}H_{59}N_5O_2$ purple crystalline solid (mp >300 °C), 40 mg, 0.04 mmol, 66%. UV−vis (CH_2Cl_2) λ_{max} (rel. inten.) 446 nm (1.000), 530 (0.074), 607 (0.021), 667 (0.004); ^{1}H NMR (500 MHz, $CDCl_3$) δ 8.99 (br.s, 4H), 8.78 (s, 2H), 8.18 (d, J = 7.9 Hz, 4H), 8.14 (d, J = 7.8 Hz, 4H), 7.75 (d, J = 7.8 Hz, 4H), 7.65 (d, J = 7.9 Hz, 4H), 7.56−7.39 (m, 7H), 3.36 (dt, J = 13.9, 6.9 Hz, 2H), 3.30 (dt, J = 13.7, 6.9 Hz, 2H), 1.65 (d, J = 6.9 Hz, 12H), 1.58 (d, J = 7.0 Hz, 12H), −2.59 (s, 2H). ^{13}C NMR (126 MHz, $CDCl_3$) δ 167.6, 150.4, 148.5, 145.8, 139.3, 139.1, 138.7, 134.8, 134.3, 133.8, 132.2, 129.1, 128.5, 128.4, 128.1, 127.9, 126.9, 126.1, 125.0, 121.4, 120.5, 118.6, 34.5, 34.1, 24.5, 24.3. IR (neat, diamond ATR): see Figure S18, SI; HRMS (ESI) m/z: $[M + H]^+$ Calcd for $C_{68}H_{60}N_5O_2$ 978.4747; Found 978.4746. MS (MALDI-TOF) m/z: 977.424 $[M]^+$.

DOI: 10.1021/acs.joc.5b01906
J. Org. Chem. 2015, 80, 12076−12087

Procedure for the Synthesis of Dibromoporphyrins 7d. Monobenzoporphyrin **6d** (48 mg, 0.05 mmol) and *N*-bromosuccinimide (22 mg, 0.12 mmol) was dissolved in dry chloroform. The mixture was reflux for 6h. Reaction completion was monitored with UV−vis spectroscopy. After completion of the reaction, mixture was washed with solution of NaOH, water and brine. Organic layer was removed under vacuum and recrystallized in CH_2Cl_2/MeOH to obtain the pure compound **7d**.

*12,13-Dibromo[5,10,15,20-tetrakis[4-(1-methylethyl)phenyl]-porphinato[2,3-f] isoindole-1,3(2H)-dione, 2-phenyl (**7d**).* $C_{68}H_{57}Br_2N_5O_2$ brown solid (mp >280 °C), 55 mg, 0.048 mmol, 95%. UV−vis (CH_2Cl_2) λ_{max} (rel. inten.) 452 nm (1.000), 540 (0.061), 616 (0.014), 685 (0.011); ^{1}H NMR (500 MHz, $CDCl_3$) δ 8.90 (d, J = 4.3 Hz, 2H), 8.84 (d, J = 4.0 Hz, 2H), 8.21−8.09 (m, 8H), 7.75 (d, J = 7.7 Hz, 4H), 7.67 (d, J = 7.6 Hz, 4H), 7.54−7.37 (m, 7H), 3.56−3.18 (m, 4H), 1.63 (d, J = 6.9 Hz, 12H), 1.56 (d, J = 6.9 Hz, 12H), −2.58 (s, 2H). ^{13}C NMR (126 MHz, $CDCl_3$) δ 167.3, 150.6, 149.7, 149.5, 147.7, 145.5, 140.6, 139.4, 138.6, 138.3, 135.4, 134.1, 129.6, 129.1, 128.8, 128.3, 127.9, 126.8, 126.2, 125.6, 124.5, 121.3, 120.24 118.7, 34.5, 34.2, 24.5, 24.4. IR (neat, diamond ATR): see Figure S19, SI; HRMS (ESI) m/z: $[M + H]^+$ Calcd for $C_{68}H_{58}Br_2N_5O_2$ 1136.2937; Found 1136.2984. MS (MALDI-TOF) m/z: 1136.222 $[M + H]^+$.

General Procedures for the Synthesis of Substituted Dibenzoporphyrins Were Used To Synthesize Compound 4d from 7d. *5,10,15,20-Tetrakis[4-(1-methylethyl)phenyl]-12^2,12^3-bis-(4-methoxyphenyl)benzo[b]porphinato[2,3-f]isoindole-1,3(2H)-dione, 2-phenyl (**4d**).* $C_{86}H_{73}N_5O_4$ purple crystalline solid (mp >300 °C), 10 mg, 0.008 mmol, 31%. UV−vis (CH_2Cl_2) λ_{max} (log ε) 401 nm (4.66), 460 (5.61), 540 (4.36), 579 (4.45), 616 (4.15). ^{1}H NMR (500 MHz, $CDCl_3$) δ 8.93 (d, J = 4.4 Hz, 2H), 8.84 (d, J = 4.4 Hz, 2H), 8.23−8.11 (m, 8H), 7.75 (d, J = 7.6 Hz, 4H), 7.67 (d, J = 7.6 Hz, 4H), 7.47 (dt, J = 15.7, 7.4 Hz, 7H), 7.20 (s, 2H), 6.98 (d, J = 8.3 Hz, 4H), 6.76 (d, J = 8.4 Hz, 4H), 3.83 (s, 6H), 3.36 (dt, J = 13.7, 6.8 Hz, 2H), 3.29−3.17 (dt, J = 13.7, 6.8 Hz, 2H), 1.64 (d, J = 6.9 Hz, 12H), 1.50 (d, J = 6.9 Hz, 12H), −2.44 (s, 2H). ^{13}C NMR (126 MHz, $CDCl_3$) δ 167.6, 158.1, 151.8, 151.2, 150.3, 149.4, 147.7, 146.6, 145.1, 140.8, 140.0, 139.5, 139.1, 138.5, 138.3, 134.7, 133.8, 133.7, 132.3, 131.1, 129.1, 128.2, 128.2, 127.4, 126.9, 126.1, 126.0, 120.2, 119.4, 118.3, 113.3, 55.2, 34.5, 34.2, 24.5, 24.3. IR (neat, diamond ATR): see Figure S17, SI; HRMS (ESI) m/z: $[M + H]^+$ Calcd for $C_{86}H_{74}N_5O_4$ 1240.5741; Found 1240.5794. MS (MALDI-TOF) m/z: 1239.561 $[M]^+$.

General Procedure for the Synthesis of Zinc Dibenzoporphyrins Was Used To Synthesize Compound 5d from 4d. *5,10,15,20-Tetrakis[4-(1-methylethyl)phenyl]-12^2,12^3-bis(4-methoxyphenyl)benzo[b]porphinato[2,3-f]isoindole-1,3(2H)-dione, 2-Phenyl (**5d**).* $C_{86}H_{71}N_5O_4Zn$ green crystalline solid (mp >300 °C), 10 mg, 0.007 mmol, 93%. UV−vis ($CHCl_3$) λ_{max} (log ε) 406 nm (4.32), 474 (5.35), 593 (4.17), 617 (3.95). ^{1}H NMR (500 MHz, $CDCl_3$) δ 8.99 (d, J = 4.4 Hz, 2H), 8.89 (d, J = 4.5 Hz, 2H), 8.13 (d, J = 7.6 Hz, 8H), 7.75 (d, J = 7.8 Hz, 4H), 7.67 (d, J = 7.6 Hz, 4H), 7.64 (s, 2H), 7.58−7.45 (m, 5H), 7.42 (s, 2H), 7.03 (d, J = 8.3 Hz, 4H), 6.79 (d, J = 8.1 Hz, 4H), 3.85 (s, 6H), 3.45−3.33 (m, 2H), 3.32−3.22 (m, 2H), 1.67 (d, J = 6.9 Hz, 12H), 1.52 (d, J = 6.6 Hz, 12H). ^{13}C NMR (126 MHz, $CDCl_3$) δ 167.8, 158.0, 151.6, 149.8, 149.7, 148.8, 146.1, 143.1, 143.0, 141.0, 140.6, 139.5, 137.9, 135.7, 134.8, 133.3, 133.2, 131.8, 131.2, 131.0, 129.0, 127.1, 126.99, 126.95, 125.6, 125.5, 120.8, 120.1, 118.7, 113.3, 55.2, 34.5, 34.2, 24.6, 24.4. IR (neat, diamond ATR): see Figure S23, SI; HRMS (MALDI-TOF) m/z: $[M]^+$ Calcd for $C_{86}H_{71}N_5O_4Zn$ 1301.4798; Found 1301.2712 (see SI for isotopic spectrum). MS (MALDI-TOF) m/z: 1301.507 $[M]^+$.

■ ASSOCIATED CONTENT

Supporting Information

The Supporting Information is available free of charge on the ACS Publications website at DOI: 10.1021/acs.joc.5b01906.

^{1}H NMR, ^{13}C NMR spectroscopic data, MALDI data, X-ray crystallography data, UV−vis absorption data, fluorescence data, IR spectroscopic data and computational data. (PDF)

CIF files of data (CIF)

■ AUTHOR INFORMATION

Corresponding Authors

*E-mail: kkadish@uh.edu

*E-mail: wangh3@miamioh.edu.

Notes

The authors declare no competing financial interest.

■ ACKNOWLEDGMENTS

The U.S. Department of Energy, Office of Science, Basic Energy Sciences (DE-FG02-13ER46976) supported research conducted at Miami University and the Robert A. Welch Foundation (K.M.K., Grant E-680) supported research conducted at the University of Houston. C.J.Z. acknowledges the National Science Foundation (CHE-0840446) for funds used to purchase the diffractometer used in this work. The National Science Foundation (CHE0839233) is acknowledged for providing funds to purchase the MALDI TOF mass spectrometer used in this work.

■ REFERENCES

(1) Verbiest, T.; Houbrechts, S.; Kauranen, M.; Clays, K.; Persoons, A. *J. Mater. Chem.* **1997**, *7*, 2175.

(2) Senge, M. O.; Fazekas, M.; Notaras, E. G. A.; Blau, W. J.; Zawadzka, M.; Locos, O. B.; Ni Mhuircheartaigh, E. M. *Adv. Mater.* **2007**, *19*, 2737.

(3) Tanaka, T.; Osuka, A. *Chem. Soc. Rev.* **2015**, *44*, 943.

(4) Kato, S.; Diederich, F. *Chem. Commun.* **2010**, *46*, 1994.

(5) Imahori, H.; Umeyama, T.; Ito, S. *Acc. Chem. Res.* **2009**, *42*, 1809.

(6) Yella, A.; Lee, H.-W.; Tsao, H. N.; Yi, C.; Chandiran, A. K.; Nazeeruddin, M. K.; Diau, E. W.-G.; Yeh, C.-Y.; Zakeeruddin, S. M.; Grätzel, M. *Science* **2011**, *334*, 629.

(7) Li, L. L.; Diau, E. W. *Chem. Soc. Rev.* **2013**, *42*, 291.

(8) Higashino, T.; Imahori, H. *Dalton Trans.* **2015**, *44*, 448.

(9) Urbani, M.; Gratzel, M.; Nazeeruddin, M. K.; Torres, T. *Chem. Rev.* **2014**, *114*, 12330.

(10) Zhang, M.-D.; Zhang, Z.-Y.; Bao, Z.-Q.; Ju, Z.-M.; Wang, X.-Y.; Zheng, H.-G.; Ma, J.; Zhou, X.-F. *J. Mater. Chem. A* **2014**, *2*, 14883.

(11) Yi, C.; Giordano, F.; Cevey-Ha, N. L.; Tsao, H. N.; Zakeeruddin, S. M.; Gratzel, M. *ChemSusChem* **2014**, *7*, 1107.

(12) Yella, A.; Mai, C. L.; Zakeeruddin, S. M.; Chang, S. N.; Hsieh, C. H.; Yeh, C. Y.; Gratzel, M. *Angew. Chem., Int. Ed.* **2014**, *53*, 2973.

(13) Mathew, S.; Yella, A.; Gao, P.; Humphry-Baker, R.; Curchod, B. F.; Ashari-Astani, N.; Tavernelli, I.; Rothlisberger, U.; Nazeeruddin, M. K.; Grätzel, M. *Nat. Chem.* **2014**, *6*, 242.

(14) Luo, J.; Xu, M.; Li, R.; Huang, K. W.; Jiang, C.; Qi, Q.; Zeng, W.; Zhang, J.; Chi, C.; Wang, P.; Wu, J. *J. Am. Chem. Soc.* **2014**, *136*, 265.

(15) Lu, J.; Xu, X.; Cao, K.; Cui, J.; Zhang, Y.; Shen, Y.; Shi, X.; Liao, L.; Cheng, Y.; Wang, M. *J. Mater. Chem. A* **2013**, *1*, 10008.

(16) Hayashi, H.; Touchy, A. S.; Kinjo, Y.; Kurotobi, K.; Toude, Y.; Ito, S.; Saarenpaa, H.; Tkachenko, N. V.; Lemmetyinen, H.; Imahori, H. *ChemSusChem* **2013**, *6*, 508.

(17) Wang, C.-L.; Lan, C.-M.; Hong, S.-H.; Wang, Y.-F.; Pan, T.-Y.; Chang, C.-W.; Kuo, H.-H.; Kuo, M.-Y.; Diau, E. W.-G.; Lin, C.-Y. *Energy Environ. Sci.* **2012**, *5*, 6933.

(18) Ripolles-Sanchis, T.; Guo, B. C.; Wu, H. P.; Pan, T. Y.; Lee, H. W.; Raga, S. R.; Fabregat-Santiago, F.; Bisquert, J.; Yeh, C. Y.; Diau, E. W. *Chem. Commun.* **2012**, *48*, 4368.

(19) Warnan, J.; Favereau, L.; Meslin, F.; Severac, M.; Blart, E.; Pellegrin, Y.; Jacquemin, D.; Odobel, F. *ChemSusChem* **2012**, *5*, 1568.

(20) Seo, K. D.; Lee, M. J.; Song, H. M.; Kang, H. S.; Kim, H. K. *Dyes Pigm.* **2012**, *94*, 143.

(21) Panda, M. K.; Sharma, G. D.; Justin Thomas, K. R.; Coutsolelos, A. G. *J. Mater. Chem.* **2012**, *22*, 8092.
(22) Ball, J. M.; Davis, N. K. S.; Wilkinson, J. D.; Kirkpatrick, J.; Teuscher, J.; Gunning, R.; Anderson, H. L.; Snaith, H. J. *RSC Adv.* **2012**, *2*, 6846.
(23) Kurotobi, K.; Toude, Y.; Kawamoto, K.; Fujimori, Y.; Ito, S.; Chabera, P.; Sundstrom, V.; Imahori, H. *Chem. - Eur. J.* **2013**, *19*, 17075.
(24) Chen, J.; Li, K.-L.; Guo, Y.; Liu, C.; Guo, C.-C.; Chen, Q.-Y. *RSC Adv.* **2013**, *3*, 8227.
(25) Di Carlo, G.; Orbelli Biroli, A.; Pizzotti, M.; Tessore, F.; Trifiletti, V.; Ruffo, R.; Abbotto, A.; Amat, A.; De Angelis, F.; Mussini, P. R. *Chem. - Eur. J.* **2013**, *19*, 10723.
(26) Deshpande, R.; Jiang, L.; Schmidt, G.; Rakovan, J.; Wang, X.; Wheeler, K.; Wang, H. *Org. Lett.* **2009**, *11*, 4251.
(27) Vicente, M. G. H.; Jaquinod, L.; Khoury, R. G.; Madrona, A. Y.; Smith, K. M. *Tetrahedron Lett.* **1999**, *40*, 8763.
(28) Chen, Q.-Y.; Guo, C.-C.; Li, K.-L. *Synlett* **2009**, *2009*, 2867.
(29) Chumakov, D. E.; Khoroshutin, A. V.; Anisimov, A. V.; Kobrakov, K. I. *Chem. Heterocycl. Compd.* **2009**, *45*, 259.
(30) Crossley, M. J.; Burn, P. L.; Chew, S. S.; Cuttance, F. B.; Newsom, I. A. *J. Chem. Soc., Chem. Commun.* **1991**, 1564.
(31) Jaquinod, L.; Khoury, R. G.; Shea, K. M.; Smith, K. M. *Tetrahedron* **1999**, *55*, 13151.
(32) Ono, N.; Yamada, H.; Okujima, T. *Handbook of Porphyrin Science*; World Scientific: Singapore, 2010; Vols. *1*−*5*.
(33) Carvalho, C. M.; Brocksom, T. J.; de Oliveira, K. T. *Chem. Soc. Rev.* **2013**, *42*, 3302.
(34) Smith, K. M.; Lee, S. H.; Vicente, M. G. a. H. *J. Porphyrins Phthalocyanines* **2005**, *9*, 769.
(35) Lash, T. D. *J. Porphyrins Phthalocyanines* **2001**, *5*, 267.
(36) Ojadi, E. C. A.; Linschitz, H.; Gouterman, M.; Walter, R. I.; Lindsey, J. S.; Wagner, R. W.; Droupadi, P. R.; Wang, W. *J. Phys. Chem.* **1993**, *97*, 13192.
(37) Ermilov, E. A.; Tannert, S.; Werncke, T.; Choi, M. T. M.; Ng, D. K. P.; Röder, B. *Chem. Phys.* **2006**, *328*, 428.
(38) Peychal-Heiling, G.; Wilson, G. S. *Anal. Chem.* **1971**, *43*, 545.
(39) Lanese, J. G.; Wilson, G. S. *J. Electrochem. Soc.* **1972**, *119*, 1039.
(40) Fang, Y.; Gorbunova, Y. G.; Chen, P.; Jiang, X.; Manowong, M.; Sinelshchikova, A. A.; Enakieva, Y. Y.; Martynov, A. G.; Tsivadze, A. Y.; Bessmertnykh-Lemeune, A.; Stern, C.; Guilard, R.; Kadish, K. M. *Inorg. Chem.* **2015**, *54*, 3501.

DOI: 10.1021/acs.joc.5b01906
J. Org. Chem. 2015, 80, 12076−12087